ADVANCED FUNCTIONAL MATERIALS
www.afm-journal.de

# Particle Surfaces to Study Macrophage Adherence, Migration, and Clearance

*Dedy Septiadi, Aaron Lee, Miguel Spuch-Calvar, Thomas Lee Moore, Giovanni Spiaggia, Wildan Abdussalam, Laura Rodriguez-Lorenzo, Patricia Taladriz-Blanco, Barbara Rothen-Rutishauser, and Alke Petri-Fink**

**Nanoparticle adsorption to substrates pose a unique challenge to understand uptake mechanisms as it involves the organization of complex cytoskeletal components by cells to perform endocytosis/phagocytosis. In particular, it is not well-understood from a cell mechanics perspective how the adhesion of particles on substrate will influence the ease of material clearance. By using a particle model, key contributing factors underlying cell adhesion on nonporous silica particle surfaces, migration and engulfment, are simulated and studied. Following a 24 h incubation period, monocyte-derived macrophages and A549 epithelial cells are able to adhere and remove particles in their local vicinity through induction of adhesive pulling arise from cell traction forces and phagocytic/endocytic mechanisms, in a size-dependent manner. It is observed that such particle-decorated surfaces can be used to address the influence of surface topography on cell behavior. Substrates which presented 480 nm silica particles are able to induce greater development and maturation of focal adhesions, which play an important role in cellular mechanoregulation. Moreover, under a chemotactic influence, in the presence of 30% fetal bovine serum, macrophages are able to uptake the particles and be directed to translocate along a concentration gradient, indicating that local mechanical effects do not substantially impair normal physiological functions.**

## 1. Introduction

Exposure to nanoparticulate materials has important ramifications for human health and disease. In order to fully understand the impact of nanomaterials on biological systems, it is important to assess cellular internalization behavior and further examine how this process alters normal physiology. Nanoparticle adsorption to medically relevant surfaces, such as implants or biological barriers (i.e., endothelial and epithelial cells), can instigate unique cellular uptake mechanisms that require complex cytoskeletal dynamics similar to those involved in pathogen (e.g., bacteria or virus) clearance by phagocytic cells, such as macrophages.[1] For free-floating objects, a phagocytic event requires physical contact (i.e., recognition) between the cell and the object, and then pushing and pulling by the cell cytoskeleton to efficiently uptake the objects.[2] In a strongly adherent particle system, this phagocytic process is however still not well understood, more specifically, from a cell mechanics point of view.

Adhesion of particles on substrates is governed by electrostatic and van der Waals forces[3–6] which depend on the physicochemical properties of particles and substrates.[7,8] It typically has a magnitude of several nanoNewton (nN).[8] Therefore, in the event of phagocytosis, it is hypothesized that macrophages must exert

Dr. D. Septiadi, A. Lee, Dr. M. Spuch-Calvar, Dr. T. L. Moore, G. Spiaggia, Dr. L. Rodriguez-Lorenzo, Dr. P. Taladriz-Blanco, Prof. B. Rothen-Rutishauser, Prof. A. Petri-Fink
Adolphe Merkle Institute
University of Fribourg
Chemin des Verdiers 4, Fribourg 1700, Switzerland
E-mail: alke.fink@unifr.ch

The ORCID identification number(s) for the author(s) of this article can be found under https://doi.org/10.1002/adfm.202002630.



**DOI: 10.1002/adfm.202002630**

Dr. W. Abdussalam
Department of High Energy Density
Helmholtz-Zentrum Dresden-Rossendorf
Bautzner Landstraße 400, Dresden 01328, Germany

Dr. L. Rodriguez-Lorenzo
Department of Life Sciences
Nano for Environment Unit
Water Quality Group
Av. Mestre José Veiga s/n, Braga 4715-330, Portugal

Prof. A. Petri-Fink
Department of Chemistry
University of Fribourg
Chemin du Musée 9, Fribourg 1700, Switzerland

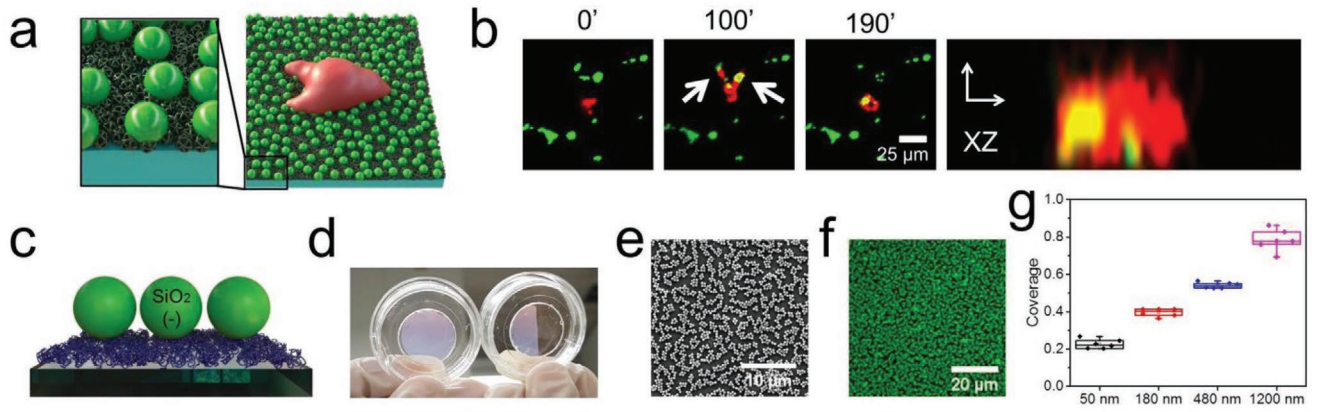


**Figure 1.** a) Illustration of clearance and migration by single macrophage (red) on particle surface (green). b) Time-lapse fluorescence images showing particle phagokinetic by single MDM (red). A single MDM and cluster of particles (1.2 µm rhodamine B-labeled silica particles, green) were initially separated by a distance of 20 µm which decreases as the MDM migrates toward the particles and eventually uptake the particles through lamellipodium/filopodium expansion (i.e., actin protrusion; white arrow; 100 min). Right panel shows the orthogonal view (XZ) of distribution of intracellular particles in MDM after 190 min. c) Graphical representation of particle surface engineered by layer-by-layer deposition. Blue color indicates cationic polymers. d) Photograph of glass bottom dish fully- (left panel) and half-decorated (right panel) with particle surfaces. e) Scanning electron and f) Fluorescence confocal micrograph of particle surface consisting 480 nm rhodamine B-labeled silica particles. g) Determination of coverage of particle surface by means of image processing. Larger particles possess higher coverage in comparison to small ones.

a greater mechanical (i.e., push and pull) force than the stabilizing adhesive force in order to detach the particles from the surface.

In the following work, we simulated adherence and phagocytic activity of primary monocyte-derived macrophages (MDMs) using a particle-presenting surface. To evaluate the consequences of size and surface charge as two of the most salient physicochemical features governing the substrate adhesion force, cellular interactions, and behavior, we generated surfaces using amorphous, nonporous, and biocompatible (rhodamine B-labeled) silica particles with sizes ranging from 50 to 1200 nm[9] through electrostatic interactions between negatively-charged colloids and a positively-charged poly(L-lysine) (PLL) coated glass surface (**Figure 1**a).[10] By using time-lapse fluorescence imaging, scanning electron, and micropillar traction force microscopy,[11] we demonstrate the ability of macrophages to adhere and migrate on the particle surface, and mechanically remove the particles in their vicinity. We further compared our results to nonphagocytic cells, namely human alveolar epithelial type II cell (A549), which naturally uptakes particles by means of endocytosis and possess strong adherence to substrates.[12–15] In particular, epithelial cells are relevant cells as they serve as the first cellular barrier to protect against translocation of particles. Given that particles are likely to encounter either an epithelial cell or a macrophage, understanding the role that adhesive forces play in relative clearance dynamics is critical to evaluating particle fate. We further confirmed that such particle-decorated surfaces could be effectively used to address open questions regarding topographical effects on cell behavior in the context of native extracellular matrix function. Finally, we investigated the possibility of concomitant phagocytic migration under chemotactic influence in the presence of 30% fetal bovine serum to preferentially control the direction of uptake and translocation.

## 2. Results and Discussion

### 2.1. Role of Protrusion Mechanics in Phagocytosis of Adsorbed Particles

MDMs were characterized and confirmed using flow cytometry measurement through the presence of surface markers associated to macrophages namely CD14 and CD163, respectively. To study whether these macrophages were able to phagocytose particles adsorbed to glass substrates, an in vitro imaging uptake experiment was conducted. Negatively-charged (rhodamine B-labeled) silica particles with a diameter of 1.2 µm (Figure S1, Supporting Information) were used as a model system. Briefly, particles were spin-coated onto a glass bottom dish and left to dry under ambient conditions before slow addition of MDMs and fresh culture medium. These spin-coated particles yielded agglomerates on the glass surface (Figure S2, Supporting Information), which was attributed to the drying effect. These clusters of particles were nonetheless stable in culture medium; no sign of particle detachment or reclustering was observed during live cell imaging (Video S1, Supporting Information). In vitro time-lapse imaging data showed that macrophages were able to migrate closely to the particle site before phagocytosing the particles (Figure 1b). This clearance process is relatively slow; particle association through filopodium/lamellipodium protrusion and engulfment was completed in ≈20–30 min (Figure 1b; and Video S1, Supporting Information). Z-stack imaging shows that membrane protrusion to assist particle internalization by pulling was applied from above the particles (Figure S3, Supporting Information). Imaging data also demonstrate that this protrusion pulling force was sufficient to pull and detach the particles from the glass substrate.

To ascertain if the adhesion of particles and substrate could influence the phagokinetic activity of MDMs, we functionalized the glass substrate with a cationic polymer, PLL, which provides

an overall positive surface charge to the glass. By taking advantage of electrostatic interaction with negatively-charged silica particles (see Zeta potential in Figure S4, Supporting Information), a similar spin-coating deposition approach[10] was employed. By using atomic force microscopy (AFM) and quartz crystal microbalance (QCM), we first checked the formation of PLL layer on the glass substrate. AFM imaging data show formation of a thin PLL film where the average thickness is around 3 nm, while QCM detects the change of quartz oscillation frequency representing the existence of film with an average thickness of ≈4.6 nm (Figures S5, S6, and Table S1, Supporting Information). Upon particle deposition, AFM data confirm an increase in height profile corresponding to the size of the particles, indicating successful functionalization of particles on PLL-coated substrate (Figure S5; see also fluorescence confocal data in Figure S2, Supporting Information). Moreover, the in vitro experiment demonstrated that MDMs were still able to pull, detach and internalize the particles on PLL-coated glass, which was expected to possess a stronger adhesion interaction (i.e., higher electrostatic interaction) than on non-PLL coated glass, in a period of 20 min (Figure S7 and Video S2, Supporting Information). This result is concordant with the expectation that the protrusion pulling force exerted by macrophages is ultimately stronger than the adhesive force between the particle and the substrate. Nevertheless, no major difference in the phagocytic rate for both cases (PLL vs non-PLL system) was observed.

### 2.2. Fabrication of Homogenous Particle Surfaces

Our ultimate objective was to simulate the adhesion of differently sized and charged particles on a substrate and then assess macrophage clearance in dependence of these parameters. We realized that by varying initial particle concentrations and deposition times, a similar layer-by-layer deposition technique[10] can be used to produce a homogenous particle surface. To fabricate this surface, we first functionalized the glass with PLL and then applied a silica suspension onto the PLL layer for 10 min, this was followed by thorough rinsing with water to remove excess particles. To study the influence of particle size on particle surface formation and topography, we synthesized four different sizes of (rhodamine B-labeled) silica particles: 50, 180, 480, and 1200 nm. Important physicochemical characterization, such as hydrodynamic diameter and Zeta potential of the particles are summarized in Figures S1 and S4 (Supporting Information). Using AFM, scanning electron and fluorescence confocal microscopy, we observed successful formation of a very homogenous, thin layer of silica particle surfaces (Figure 1d–f; and Figures S5 and S8, Supporting Information). Root mean square (Rms) roughness of surfaces describing the topography of the surfaces was identified as follows: bare glass (0.6 nm), PLL-functionalized glass (4.7 nm), 50 nm silica-functionalized (30.6 nm), 180 nm silica-functionalized (78.4 nm), 480 nm silica-functionalized (198.9 nm), and 1200 nm silica-functionalized (408.5 nm; and Table S2, Supporting Information). Larger particles generate greater topographical contrast and consequently yield surfaces with higher roughness values. Image analysis of corresponding electron micrographs shows the difference in coverage for each particle size, ranging from 22% (50 nm) to 80% (1.2 μm) with density (described as number of particles $\mu m^{-2}$) ranging from 90 particles $\mu m^{-2}$ (50 nm) to 0.5 particle $\mu m^{-2}$ (1.2 μm), respectively (Figure S9, Supporting Information). The decrease of particle density with particle size is also observed by QCM (Figure S10, Supporting Information). We show that the increase of particle density with decreasing size is governed principally by geometric packing considerations.

### 2.3. Phagocytosis/Endocytosis on Particle Surface

Phagocytic activity of macrophages on particle surfaces was evaluated by culturing MDMs for 24 h at 37 °C and 5% $pCO_2$. Postincubation, cell samples were fixed and analyzed using scanning electron and fluorescence confocal microscopy. In vitro imaging data are shown in **Figure 2**a,b. Particle association (i.e., cleared area in Figure 2a; and Figure S11, Supporting Information) was observed, indicating adhesion and internalization alongside intracellular distribution (see the 3D image reconstruction in Figure 2b) by MDMs for 180, 480, and 1200 nm particle surfaces, but no cleared region was observed for the 50 nm sample. To quantify the number of associated particles, the electron micrographs were further subjected to particle counting by measuring the cleared area. Our result depicted in Figure 2c shows that single MDMs cleared more smaller particles (180 nm; ≈5000 particles per cell) compared to large ones (1.2 μm; ≈500 particles per cell). We compared our result by incubating nonphagocytic cells, namely human alveolar epithelial type II cells (A549). Strikingly, we only observed significant particle association of 480 nm (≈3800 particles per cell) and 1200 nm (≈800 particles per cell) particles by A549 cells, but not 50 and 180 nm particles (Figure 2d; and Figure S12, Supporting Information). For the latter cases, limited particle association was observed. Moreover, in the case of 480 and 1200 nm, A549 significantly uptake more particles than MDMs, which we hypothesized was due to A549's phenotype as a strongly adhering cell line, therefore, possessing stronger traction force, allowing A549 cells to pull and easily detach the particles from PLL substrate than MDMs. To address this, we calculated the adhesion between the particle and the PLL substrate which was previously reported to consist of both electrostatic and van der Waals forces.[4] For all particle sizes, each with different Zeta potential values (Figure S3, Supporting Information) deposited on the PLL substrate with a surface charge of 60 mV,[16] the highest adhesive force calculated was 0.62 nN (for 1.2 μm; see corresponding values in Figure 2e). We further quantified the traction force (i.e., force exerted by cells on substrates) by means of a micropillar traction force assay.[11,17] By measuring the bending of pillars upon contact with cells (Figure 2f), traction force was determined. The result presented in Figure 2g shows that MDM and A549 cells possess a traction force of ≈1.2 and 2.4 nN, respectively. The measured traction force values are more than two times greater than the adhesive force associated with particle-substrate interactions, and therefore are sufficient to pull particles from the substrate. In addition, the stronger traction force of A549 cells can be further seen by monitoring the maturation of paxillin focal adhesions from which the traction force was exerted (Figure 2h). Larger focal adhesion sizes

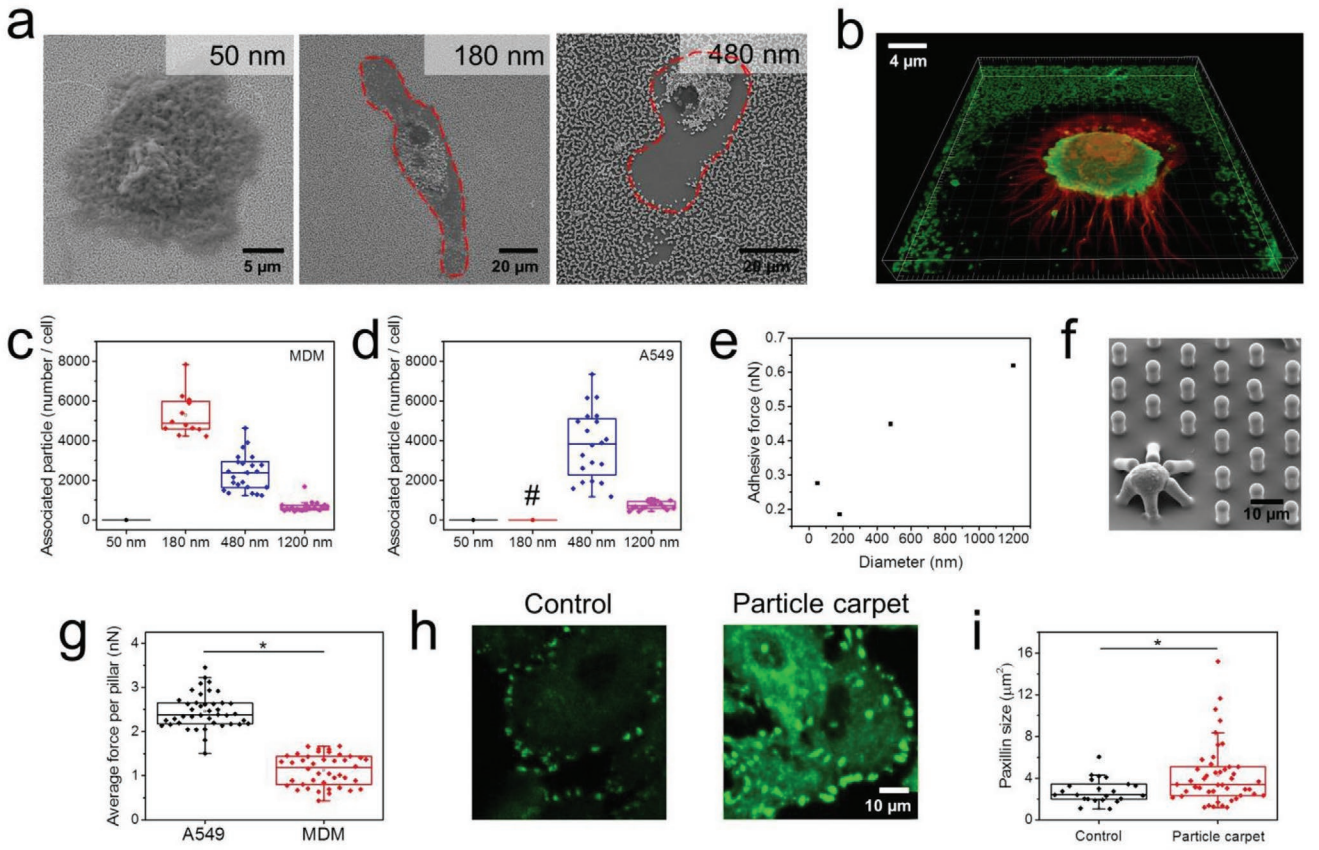


**Figure 2.** a) Representative scanning electron micrographs showing the adhesion and uptake of single MDM on particle surfaces engineered with different sizes. Particle clearance can be observed in 180 and 480 nm particle surface by analyzing cleared area on the images (see the area under red dashed line). b) A 3D-rendered fluorescence confocal micrograph of single MDM (red) clears the 480 nm particles (green) in the vicinity. Quantification of particles associated to c) MDMs and d) A549 by means of image processing. # denotes the numbers are too low to be quantified by means of image processing. e) Calculated adhesive force between particles and PLL substrate. f) SEM image shows A549 cells bend the pillars, and through measurement of the displacement of pillars from their original positions, the average force per pillars the cells generate can be measured. g) Corresponding micropillar-based traction force value. h) Confocal micrographs of paxillin focal adhesion of A549 cells culture on glass (control) and on particle surface. g) Quantification of paxillin (focal adhesion) size obtained through image processing. One-way ANOVA, $*p < 0.05$.

indicate stronger substrate adhesion[18] and are associated with topographical features generated by these particle-decorated surfaces (Figure 2i). Topographic effects are known to influence cell behavior and it has been demonstrated that rougher surfaces can be used to improve cell attachment.[19,20] It has been hypothesized that topographical features can generate local membrane changes and recruit molecules involved in adhesion and endocytosis.[21] From this perspective, the surface topography generated by particles may facilitate preferential removal of larger objects from the surface by cells.

### 2.4. Mechanics of Phagocytosis on Particle Surface

To investigate the role of mechanics (i.e., cell adhesion and traction forces) upon detachment of particles from the substrates and subsequently uptake, live cell imaging was conducted. We used the 480 nm particle surface system, as previous data indicated higher uptake with these in comparison to other sizes. In addition, their larger size also allowed easy monitoring via confocal microscopy. Time-lapse imaging data showed the dynamics of MDMs and A549 cells on particle surfaces. Both cells were observed to adhere on the particle surface and randomly migrate before performing uptake. They oscillated back and forth to facilitate the removal of particles before internalization (**Figure 3**a; and Video S3, Supporting Information). This oscillation can be seen from cell displacement data as function of time obtained by cell tracking (Figure 3b,c). In comparison with A549 cells (Video S4, Supporting Information), MDMs performed the "wiggling" movement earlier (9 vs 12 h), leading to faster particle removal. Once the particle area beneath the cells was cleared, both cells randomly change their orientation, migrate, and subsequently uptake particles via leading-edge (F-actin) protrusions. Scanning electron micrographs of the cells after 24 h confirmed the clearance orientation, which corresponds to the direction of cell migration. A high number of distributed particles were noted at the leading edge (Figure 3c,d; and Figure S12, Supporting Information) in comparison with the trailing edge of the cells (Figure 3d), as the leading edge controls the direction of migration and therefore, particle uptake. Particles were also found on the top of cells, which can be attributed to recycling of membrane protrusions

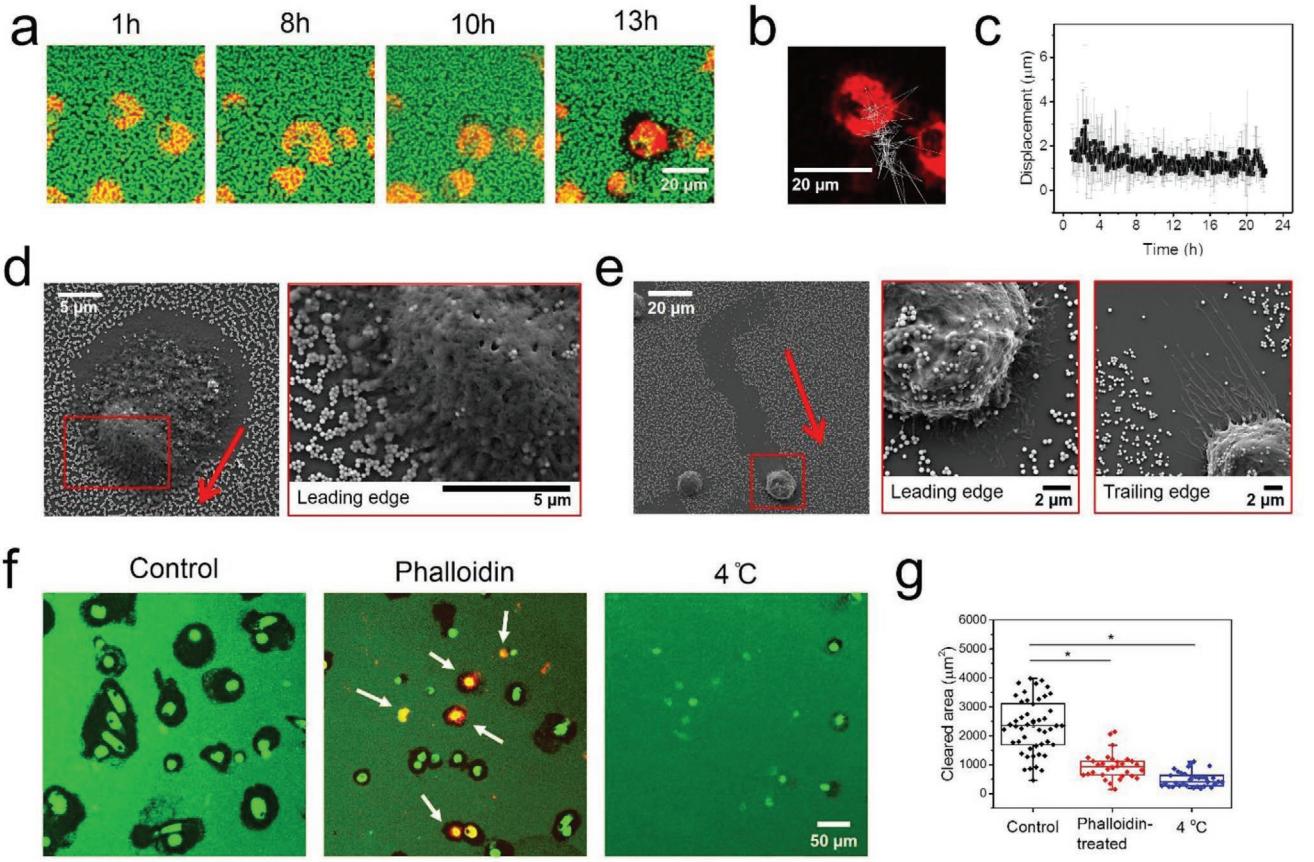


**Figure 3.** a) Time-lapse fluorescence images showing the uptake and migration of MDMs (red) on 480 nm particle surface (green). b) Trajectory of cell migration (white line) and c) average cell displacement over time. Black dots and gray lines are average value and standard deviation. Small displacement values from early time points indicates that cells do not actively move, instead they gyrate in a localized position in order to displace the particle from the surface. d) Scanning electron micrograph showing the trajectory of uptake and migration (red arrow). Red inserts show the leading edge and trailing edge of an individual d) MDM and e) A549 cell. Particles after being cleared are both observed inside and attached on the cell membranes. f) Confocal fluorescence images showing the reduction of particle clearance upon introduction of actin binding phalloidin drug and incubation at low temperature in comparison with control cells, indicating the important role of actin during particle uptake. White arrows show internalization of Alexa 488 phalloidin conjugate. g) Corresponding cleared area by single cells quantified by image processing. One-way ANOVA, $*p < 0.05$.

from the leading edge through actin or membrane ruffles[22] to the upper part of the cells (Figure 3d; and Figures S12 and S13, Supporting Information). In this upper region, phagocytosis (for MDMs) or endocytosis (for A549) is able to occur.

Dynamic formation of F-actin protrusion (lamellipodia/filopodia) is a well-known cellular process driven by both polymerization of actin monomer (G-actin) to actin filament (F-actin) and depolymerization of F-actin to G-actin, involving adenosine triphosphate (ATP) binding and ATP hydrolysis to adenosine diphosphate (ADP), respectively.[23] To understand the important role of actin polymerization/depolymerization plays in membrane protrusion formation and particle clearance, two additional experiments were conducted. Our first investigation was performed by introducing a phalloidin-based drug which is known to bind and stabilize F-actin,[24] therefore, reducing depolymerization of F-actin and disturbing the dynamics of actin organization.[25] 6 h after the cell seeding, $50 \times 10^{-9}$ M of Alexa Fluor 488 phalloidin was introduced and cells were incubated for the next 18 h before cell imaging was conducted. The internalization of phalloidin drug was successfully confirmed through the presence of F-actin staining inside the cells (Figure 3f; and Figure S14, Supporting Information). Our results demonstrate that the removal of particles, which is measured by the clearance area by phalloidin-treated cells, was impeded in comparison with control cells, which we attribute to the alteration of the actin function due to phalloidin binding to F-actin (Figure 3f,g). To highlight the importance of ATP to actin dynamics, we cultured cells at 4 °C which is known to affect endocytic and phagocytic behaviors as well as cellular metabolism and functions.[26,27] Previous results have demonstrated reduction of particle uptake in an in vitro suspension scenario.[28] Our results confirm that at low temperatures normally used to arrest metabolic activity and consequently phagocytosis, particle clearance was also inhibited (Figure 3f,g), highlighting that observed particle clearance is indeed an actin dependent process.

Based on these important findings, we propose a mechanism of particle clearance by adherent cells which is summarized in **Figure 4**a,b. The clearance is strongly dependent on the particle location: to remove particles beneath the cells, cells adhere, and perform the wiggling (oscillation; Figure 4a, step 1–2). Once the particles are detached and stick to the basal membrane, particles are internalized (Figure 4a, step 3–4). To clean particles in

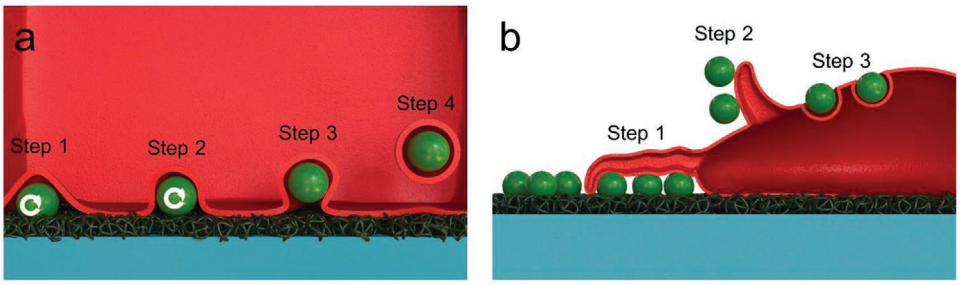


**Figure 4.** Proposed mechanism of particle clearance by adherent cells. The clearance is depending on the location of particles: a) beneath the cells and b) in cell vicinity. For particles beneath cells, by oscillating back and forth (step 1–2), cells facilitate the removal of particles before being phagocytosed from the basal membrane side (step 3–4). For particles in the cell vicinity, after the basal particles are being cleared, by generating traction force through protrusion of F-actin filaments in the leading edge (pulling force, step 1), cells detach the particles. Once the particles are detached from the substrates and adhere to the cell membrane, cells eventually retract their lamellipodia/filopodia (step 2) and this membrane protrusion is recycled back into the cell (also called actin or membrane ruffle). In this region, phagocytosis (for MDM) or endocytosis (for A549) takes parts (step 3).

their vicinity after the particles underneath are already cleared, cells generate traction force through protrusion of F-actin filaments (filopodia/lamellipodia) in the leading edge (pulling force; Figure 4b, step 1, Figure S15, Supporting Information) followed by detaching the particles. Once the particles are detached from the substrates and adhered to the cell membrane, cells eventually retract their lamellipodia/filopodia (Figure 4b, step 2) and this membrane protrusion is recycled back into the cell (Figure 4b, step 3). In this region, phagocytosis (for MDM) or endocytosis (for A549) can take place. Limitation of initial contact of cells and particles in our system also hindered the possibility to shovel the particles from the bottom. Furthermore, the separation between particles and the surface is considerably small and this likely limits the ability of the cell to extend lamellipodia/fillopodia below the particle. Therefore, due to these spatial constraints, detachment, and removal of particles from the surface are more likely to occur via a vertical approach.

### 2.5. Chemotaxis on Particle Surface

To study and simulate this cell migration and clearance capacity in the presence of high chemical gradient (chemokine), which is hypothesized to take place concomitantly, we engineered particle surfaces on a permeable cell culture insert, which are typically used to study vertical cell transmigration and chemotaxis (**Figure 5**a).[29] Fluorescence confocal micrographs shown in Figure 5b indicate the successful fabrication of 480 nm particle surface on the inserts. It is important to note that, the pores of the inserts are not blocked by the particles, thereby allowing the cells to pass through. The chemotaxis procedure was performed in the following manner: MDMs, which were previously starved in serum-free medium at 37 °C and 5% $pCO_2$ (for a minimum period of 6 h prior to the experiment) were seeded and cultured in fresh, serum-free medium on the apical (top) side of the surface while high concentrations of chemokines (30% fetal bovine serum, FBS) were added to the basal (bottom) side of the inserts (Figure 5a). Post-24 h of incubation, cells were fixed, fluorescently-labeled, and analyzed using z-stack fluorescence microscopy. A corresponding orthogonal view of the z-stack image is shown in Figure S16 (Supporting Information). On the apical side, a few MDMs were observed to clear particles in their vicinity (Figure 5c). On the basal side, by counting the transmigratory cells, we confirmed more than 40% of MDMs had translocated while carrying their particle cargo (Figure 5d). This finding confirms that both chemotaxis and particle clearance can indeed take place in parallel and local mechanical effects due to particle uptake do not substantially impair normal physiological function.

## 3. Conclusion

In summary, particles-presenting surfaces were successfully fabricated through electrostatic-driven assembly. The adhesion of the silica particle to the substrate (<0.6 nN) is controlled by

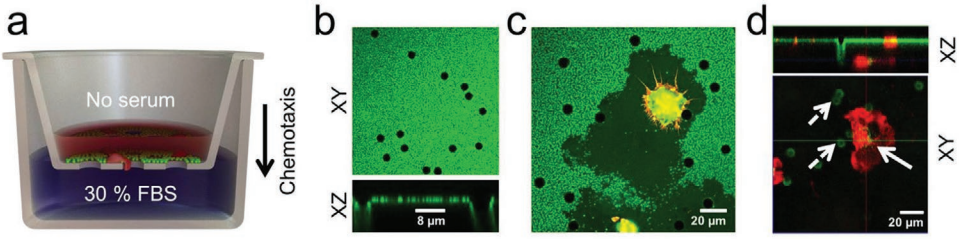


**Figure 5.** a) Illustration of particle clearance and chemotaxis on particle surface. b) Confocal micrograph showing successful fabrication of particle surface on permeable inserts. Black holes in panel b) represent the insert pores with 8 µm in diameter. Concomitant uptake and chemotaxis by MDM in the presence of chemoattractant is observed. c) Particle clearance by MDM (red) on the apical (top side) of the inserts. A single MDM is able to clear particles in the vicinity upon migrating to the basal side containing 30% FBS. d) Single MDM after clearing the particles on the apical side move and translocate to basal side (bottom). Solid arrows show pore of the insert while dashed arrows resemble intracellular particles in the basal side.

varying the particle size and surface charge. We have shown that primary macrophages (MDMs) and epithelial cells (A549) are able to adhere on the particle surface and slowly remove the particles in their vicinity. Our result also highlights the important role of adhesive pulling forces (i.e., traction force) and filopodium/lamellipodium protrusions exerted by cells through F-actin and focal adhesions to mechanically detach particles from substrates. We also confirm that both chemotaxis and particle clearance by cells can coexist. The results presented here provide important knowledge of one aspect of host defense against foreign objects as well as offer insights into cellular recognition of artificial substrates. We have shown that the interaction with particle surfaces bears many similarities with those observed to occur on topographically defined interfaces and may offer a route to designing interactive biointerfaces.

## 4. Experimental Section

*Silica Particle Synthesis and Characterization*: Four different sizes of silica particles were synthesized following the Stöber method[30] as previously described in literature.[31,32] Initially, 5.28 mg (9.8 µmol) of the fluorophore rhodamine B isothiocyanate (RhoB; Sigma-Aldrich, Germany) dissolved at 10 mg $mL^{-1}$ in ethanol was mixed with 7.5 µL (32.1 µmol) of (3-aminopropyl)triethoxysilane (APTES; Sigma-Aldrich, Germany) and left to stir overnight. The RhoB-APTES conjugate was then used without further purification. For small size particles (50 nm), 22 mL of the silica precursor (i.e., tetraethyl orthosilicate, TEOS; Sigma-Aldrich, Germany) was added to a preheated (60 °C) mixture of 208 mL of ethanol, 13.5 mL of deionized water and 7.8 mL of ≈25% ammonium hydroxide (Sigma-Aldrich, Germany). After 1 min of core formation, 300 µL of the RhoB-APTES solution was added to the mixture to form fluorescently-labeled silica layers around these initially formed particle cores. The reaction was further stirred overnight and purified by centrifugation at 5000 g and washed with ethanol three times, followed by redispersion in autoclaved Milli-Q water followed by three rinsing cycles. 180 nm $SiO_2$ particles were synthesized in the same fashion as the 50 nm particles, but by altering the reagent ratios: 11 mL TEOS, 180 mL ethanol, 36 mL of deionized water, and 24 mL 25% ammonium hydroxide. Likewise, 400 nm silica particles were synthesized with ratios of 45 mL TEOS, 348 mL ethanol, 27 mL of deionized water, and 81.8 mL of 25% ammonium hydroxide. For larger (1.2 µm) particles,[9] 2 mL of TEOS was added dropwise (2 mL $h^{-1}$) at room temperature to a mixture of 75 mL of isopropanol, 25 mL of methanol, and 21 mL of ammonium hydroxide. After 1 h of core formation, premixed solutions of TEOS (6 mL) and APTES rhodamine B isothiocyanate (300 µL) were added dropwise (2 mL $h^{-1}$) to the reaction mix. The reaction was further stirred overnight and purified by centrifugation at 100 g and washed twice with ethanol followed by redispersion in autoclaved Milli-Q water followed by three rinsing cycles. The synthesized particles were then visualized using a transmission electron microscope (FEI Tecnai Spirit, US) and their corresponding size was determined using FIJI software (NIH, US). The hydrodynamic diameter and zeta potential were measured by dynamic light scattering and zeta potential analyzer (Brookhaven, US), respectively. The particle concentration was determined by measuring the weight of 2 mL of particle suspension after evaporating the water at 50 °C.

*Cell Culture*: Human blood MDMs were isolated from buffy coat suspensions provided by the blood donation service, SRK Bern. The cells were purified using CD14 Microbeads (Milteny Biotech, Germany) following the procedure reported previously.[33] The macrophages were seeded in 6 well-plates (Thermo Fisher Scientific, Germany) in cell culture media containing RPMI 1640 (Gibco, Life Technologies Europe B.V., Zug, Switzerland) supplemented with 10% v/v fetal bovine serum (FBS; PAA Laboratories, Chemie Brunschwig AG, Basel, Switzerland), 1% v/v L-Glutamine (Life Technologies Europe), and 1% v/v penicillin/streptomycin (Gibco) and kept in a humidified incubator (37 °C, 5% $pCO_2$) for 1 week. Human alveolar type II epithelial cells (A549) were purchased from the American Type Culture Collection (ATCC, US) and cultured in complete cell culture medium at 37 °C with 5% $pCO_2$ for 48–72 h until reaching 90% cell confluency.

*Particle Uptake Experiments*: 100 µL of 1.2 µm silica particles (with concentration 20 µg $mL^{-1}$) were spin coated on sterile glass bottom dish (Mattek, US) and left to dry at room temperature overnight. ≈20 000 MDMs which were previously stained using Vybrant DiD (Invitrogen, Germany) following the protocols provided by manufacturers were seeded on the dish. Next, 2 mL of culture medium was added gently into the dish. Cells were monitored through fluorescence live cell imaging at 37 °C and 5% $pCO_2$ using fluorescence LSM microscope setup, Zeiss LSM 710 (Zeiss, Germany).

*Fabrication of Particle Surface*: Particle surfaces consisting four different sizes of silica particles were fabricated by means of layer-by-layer deposition technique.[10] Briefly, glass bottom dishes (Mattek, US) possessing negative surface were conditioned with positive charge (cationic) PLL (Sigma-Aldrich, 0.1% w/v in $H_2O$ for 5 min followed by three rinses with 1 mL of Milli-Q water). Next, 400 µL of silica suspension of different sizes (concentration 10 mg $mL^{-1}$) were applied for 5 min. After rinsing, the nonattached particles were removed and the surfaces were washed with Milli-Q water ten times to ensure only attached particles were present. The surfaces were left to dry at room temperature before cell experiments were conducted. All the surfaces were analyzed using a scanning electron microscope (SEM) Tescan Mira3 LM FE (Tescan, US), atomic force microscope and fluorescence LSM setup.

*Atomic Force Microscopy Measurement*: Samples were imaged using an atomic force microscope (NX10, Park Systems, South Korea) in tapping mode in air. Images were obtained using aluminum-coated silicon probes (TAP300Al-G, Budget Sensors, Bulgaria) with a nominal resonant frequency of 300 kHz and a force constant of 40 N $m^{-1}$. An area of $5 \times 5$ $\mu m^2$ was scanned for all particles.

*QCM Characterization of PLL Layer and Particle Adsorption*: 10 MHz quartz sensor crystals (openQCM by Novaetech S.r.l., Cod: AT10-14-6-UP) were cleaned by immersion in 2% Hellmanex II solution for 30 min followed by rinsing with water and ethanol to remove any surface contaminants. Cleaned sensors were mounted in the sensor module and calibrated before use. Frequency data were recorded for bare crystals before surface conditioning with 1 mg $mL^{-1}$ PLL solution for 10 min. Excess polymer was rinsed from the surface and the sensor was dried under vacuum before being remounted to ascertain the frequency change associated with adsorption of polyelectrolyte. Similarly, silica adsorption was performed on crystals treated with PLL for 10 min before removal of the excess through rinsing and determination of the frequency response associated with particle attachment. Each frequency response was allowed to thermally equilibrate before commencing data acquisition for 5 min.

*Quantification of Particle Surface*: The coverage and density of particle surfaces were measured by means of particle counting using Fiji software (NIH, US). Briefly, particles on the SEM images with the size of $10 \times 10$ $\mu m^2$ were counted individually. The coverage was determined by dividing the obtained numbers with the theoretical maximum number of particles allowed in a 100 $\mu m^2$ area.

*Calculation of Adhesive Force*: The adhesive forces which consist of electrostatic force and van der Waals interactions are calculated based on the following literature.[5,6] Briefly, the calculation steps are described as follows: i) The electrostatic interaction between the PLL substrate and the silica particles is given by their charges, $q_s = 4\pi\varepsilon_0\phi_s r_s$ and $q_p = 4\pi\varepsilon_0\phi_p r_p$ for substrate and particles, respectively. Next, the electrostatic interactions ($F$) are calculated using the following equation

$$F = \frac{1}{4\pi\varepsilon_0\varepsilon_w}\frac{q_s q_p}{r_d^2} \quad (1)$$

where $r_d$ denotes a distance between cationic polymer and the silica. For PLL surface potential, $\phi_s$ = 60 mV, Zeta potential of particles obtained through the measurement (e.g., for 50 nm), $\phi_p$ = –32.09 mV, permittivity,

$\varepsilon_0$ = 8.854 187 817 × $10^{-12}$ $C^2$ $N^{-1}$ $m^{-2}$, $\varepsilon_w$ = 78.5 $C^2$ $N^{-1}$ $m^{-2}$, distance range $r_s$ = $10^{-6}$ nm, and $r_p$ = $10^{-7}$ nm, and approximated $r_d$ = $10^{-9}$ nm yields electrostatic forces $F \approx -0.27$ nN, in which the negative value represents attractive interaction. ii) van der Waals forces ($F_{vdw}$) based on Lifshitz theory[34] are calculated using the following equation

$$F_{vdw} = \frac{AR_p}{6r_d} \tag{2}$$

where $R_p$ denotes radius of silica particles and A denotes Hamaker constant which is defined as

$$A \simeq \frac{3}{4}k_B T\frac{\varepsilon_1-\varepsilon_3}{\varepsilon_1+\varepsilon_3}\frac{\varepsilon_2-\varepsilon_3}{\varepsilon_2+\varepsilon_3}+\frac{3h\nu_e}{8\sqrt{2}}\frac{\left(n_1^2-n_3^2\right)\left(n_2^2-n_3^2\right)}{\sqrt{n_1^2+n_3^2}\sqrt{n_2^2+n_3^2}\left[\sqrt{n_1^2+n_3^2}+\sqrt{n_2^2+n_3^2}\right]} \tag{3}$$

where $k_B$, $\varepsilon_i$, $\nu_e$, and $n_i$ denote Boltzman constant, permittivity, natural frequency, and refractive index respectively. Subindices (*i*) 1, 2, 3 refer to PLL, particles, and water, respectively. iii) The total adhesive force (*W*), therefore is the sum of electrostatic and van der Waals forces

$$W = F + F_{vdw} \tag{4}$$

As an example, for silica 50 nm with $\phi_p$ = −32.09 mV, $\varepsilon_1$ = 83, $\varepsilon_2$ = 3.9, $\varepsilon_3$ = 78.58, $n_1$ = 1.37, $n_2$ = 1.46, and $n_3$ = 1.3325, natural frequency $\nu_e$ = 1 GHz, $k_B$ = 1.38 064 852 × $10^{-23}$ $m^2$ $kgs^{-2}$ $K^{-1}$, the temperature $T$ = 298.14 K, and Planck constant $h$ = 6.62 607 004 × $10^{-34}$ $m^2$ kg $s^{-1}$ (all the values are obtained from ref. [35]) yield the adhesive force with magnitude of 0.273 nN. The aforementioned calculations are repeated for other silica particles: silica 180 with $\phi_p$ = −21.37 mV, silica 480 with $\phi_p$ = −52.42 mV, and silica 1200 with $\phi_p$ = −72.5 mV.

*Cellular Uptake on Particle Surfaces*: ≈50 000 of either MDMs or A549 cells were seeded on particle surfaces following the addition of 2 mL of fresh culture media. For live cell imaging experiments, cells (previously stained using Vybrant DiD) were allowed to adhere for 1 h inside the incubator, before the samples were monitored using LSM live cell imaging. Images of samples were acquired using z-stack and time-lapse mode. For fixed cell imaging, after 24 h of incubation, cells were fixed with 4% paraformaldehyde (PFA) in phosphate-buffered saline (PBS) 1 × and followed by immunofluorescence staining. The cells were washed twice with PBS and rinsed in 0.1% Triton X-100 (Sigma-Aldrich) in PBS for 5 min and subsequently in 1% BSA (Sigma-Aldrich, Germany) in PBS for another 20 min. Rabbit monoclonal anti-Paxillin antibody (abcam, Germany) was incubated following the protocols provided by the company for 1 h and followed by addition of goat antirabbit DY488 secondary antibody (Thermo Fisher Scientific, Germany) for 25 min for visualization of paxillin focal adhesions. Cells were washed three times and the cover slips were mounted onto glass slides for microscopy measurements. For SEM imaging, after 24 h of incubation, cells were fixed with 4% PFA in 1 × PBS. Samples were dried at room temperature for 1 day before being sputtered with gold (3–4 nm in thickness) for SEM visualization.

*Fluorescence Imaging*: All of the fluorescence images were acquired using Zeiss LSM 710 confocal laser scanning inverted microscope set up with 20 × or 63 × magnification, numerical aperture, NA, 0.8 of Zeiss LCI Plan-NEOFLUAR objective lens (Zeiss GmbH, Germany). Different fluorophores (rhodamine B and Vybrant DiD) were excited sequentially at 541 and 633 nm and their emissions were collected correspondingly by the detector with the frame size 512 pixel × 512 pixel. For live cell imaging, the image was acquired in a z-stack and in time-lapse mode with the slice thickness 1–2 µm and time between each frame 5–10 min. For fixed cell imaging, DY488 (paxillin) or Alexa Fluor 488 (F-actin) was excited using a 488 nm laser. Image processing (i.e., mean intensity projection) was carried out directly using Zen 2010 software (Zeiss GmbH, Germany). 3D rendering was performed using Imaris software (Bitplane, Switzerland). False color images were adjusted to better distinguish different types of cells and particles. Cell tracking is performed using TrackMate plugin[36] available in Fiji (NIH, US). In total displacement of 10 individual cells were recorded. Data are shown as average value and standard deviation.

*Role of Actin Polymerization/Depolymerization*: ≈20 000 of MDMs were seeded on particle surfaces (480 nm) following the addition of 1 mL of fresh culture media. After 6 h of incubation, cells were incubated either with culture media containing 50 × $10^{-9}$ M Alexa 488 phalloidin (at 37 °C) or with drug free media at 4 °C for the next 18 h before cell imaging experiments were conducted. Control experiments were provided by incubating cells with drug free media at 37 °C. Live cells were imaged without any washing treatment. The experiments were performed in duplicate.

*Quantification of Cleared Area in Actin Study*: The cleared area per single cell was quantified manually by image processing using Fiji. The image processing algorithm followed three main steps: 1) intensity thresholding, 2) binarization, and 3) surface area calculation. Data are shown as average area and its 95% confidence interval. A parametric one-way analysis of variance (ANOVA) was performed. Values were considered significant (*) if $p < 0.05$.

*Quantification of Paxillin Area*: The size of paxillin focal adhesions was quantified by image processing using Fiji. The image processing algorithm followed three main steps: 1) intensity thresholding, 2) binarization, and 3) surface area calculation. Data from two conditions: A549 cells cultured on particle surface and on glass (i.e., control) is shown as average area of paxillin and its 95% confidence interval. A parametric ANOVA was performed. Values were considered significant (*) if $p < 0.05$.

*Cellular Traction Force Microscopy by Micropillar Assays*: Cell traction force exerted by MDMs and A549 cells was measured using micropillar assay developed by Microduits GmbH, Switzerland was used.[17] Briefly, 500 000 A549 cells and MDMs were cultured in a six-well plate overnight (3 wells in total). Next, 200 µL of trypsin was added for 5 min to detach the cells from the well substrate and detached cells were suspended in fresh culture media. Preparation and quantification of traction force was done by following described protocols reported in the literature.[11,17] In total, 20 000 A549 cells and MDMs in 1 mL culture media were gently added above the micropillars and grown for 24 h. Cells were fixed using 4% PFA and stained with Brilliant Cresyl Blue ALD dye (Sigma-Aldrich, Germany) for 90 s followed by 5 washes with Milli-Q water. The sample was kept in Milli-Q water and imaging was performed using a Leica DMI6000B bright field optical microscope (Leica, Germany) with a dry 40 × magnification objective (numerical aperture 0.6). Images were recorded as RGB micrographs with the frame size 1392 × 1040 pixels. Displacement of micropillars due to the force exerted by the cells were measured using Mechprofiler software developed by Microduits GmbH and calculation of the average force was based on the following literature.[17] Important physical parameters, such as length, diameter, and spring constant of the arrays which are needed for the quantification were provided by Microduits GmbH. Data were shown as average force per pillar. ANOVA was performed and values were considered significant (*) if $p < 0.05$. The measured samples were further left dried in room temperature for 1 day and sputtered with 2–3 nm gold layer for scanning electron microscopy visualization. Electron micrographs were acquired using Tescan Mira3 LM FE.

*Chemotaxis on Particle Surfaces*: Particle surfaces on Falcon Cell Culture Inserts made from polyethylene terephthalate (pore size 8 µm, culture area 0.9 $cm^2$, Thermo Fisher, Germany) were prepared in similar fashion with the glass bottom dish one. Next, 50 000 MDMs were previously starved by culturing in serum-free culture medium for 6 h before seeding on the top part (apical side) of the insert placed in 12 well plates following addition of 750 µL of free serum culture media. In the bottom part of the inserts, 1.5 mL of 30% FBS supplemented medium was added. Cells were maintained inside incubator for the next 24 h. Cells were fixed using 4% PFA in PBS and stained with Alexa Fluor 488 phalloidin (Thermo Fisher Scientific, Germany). The number of apical and basal cells was manually counted to determine the percentage of cells migrating toward the basal side.

## Supporting Information

Supporting Information is available from the Wiley Online Library or from the author.

## Acknowledgements

The authors kindly thank Hana Barosova, Dr. Roman Lehner, and Laetitia Hani for blood isolation as well as Joel Bourquin for providing 1.2 µm silica particles. They also would like to acknowledge the Swiss National Science Foundation through the National Center of Competence in Research Bio-Inspired Materials and the Adolphe Merkle Foundation for financial support for the project. D.S. also acknowledges funding from NCCR Bioinspired Materials independent grant and SPARK by Swiss National Science Foundation (190440). The work involving primary immune cells white blood cells (monocytes) isolated from human blood was approved by the committee of the Federal Office for Public Health Switzerland (Reference No. 611-1, Meldung A110635/2) for the Adolphe Merkle Institute. The datasets generated during the current study are available in the Zenodo repository, https://doi.org/10.5281/zenodo.3819724.

## Conflict of Interest

The authors declare no conflict of interest.

## Keywords

adhesion, chemotaxis, macrophage, particle surface, phagocytosis

Received: March 23, 2020
Revised: April 27, 2020
Published online:

[1] F. Castellano, P. Chavrier, E. Caron, *Semin. Immunol.* **2001**, *13*, 347.
[2] S. Schuerle, I. A. Vizcarra, J. Moeller, M. S. Sakar, B. Özkale, A. M. Lindo, F. Mushtaq, I. Schoen, S. Pané, V. Vogel, B. J. Nelson, *Sci. Rob.* **2017**, *2*, eaah6094.
[3] D. S. Rimai, D. J. Quesnel, *J. Adhes.* **2002**, *78*, 413.
[4] R. A. Bowling, in *Particles on Surfaces 1: Detection, Adhesion, and Removal* (Ed.: K. L. Mittal), Springer, Boston, MA **1988**, p. 129.
[5] F. L. Leite, C. C. Bueno, A. L. Da Roz, E. C. Ziemath, O. N. Oliveira, *Int. J. Mol. Sci.* **2012**, *13*, 12773.
[6] S. N. Ramakrishna, P. C. Nalam, L. Y. Clasohm, N. D. Spencer, *Langmuir* **2013**, *29*, 175.
[7] H. Kweon, S. Yiacoumi, C. Tsouris, *Colloids Surf. A* **2015**, *481*, 583.
[8] M. Götzinger, W. Peukert, *Powder Technol.* **2003**, *130*, 102.
[9] D. Septiadi, J. Bourquin, E. Durantie, A. Petri-Fink, B. Rothen-Rutishauser, *Sci. Rep.* **2018**, *8*, 9861.
[10] G. Decher, J.-D. Hong, *Makromol. Chem., Macromol. Symp.* **1991**, *46*, 321.
[11] D. Septiadi, W. Abdussalam, L. Rodriguez-Lorenzo, M. Spuch-Calvar, J. Bourquin, A. Petri-Fink, B. Rothen-Rutishauser, *Adv. Mater.* **2018**, *30*, 1806181.
[12] R. C. Stearns, J. D. Paulauskis, J. J. Godleski, *Am. J. Respir. Cell Mol. Biol.* **2001**, *24*, 108.
[13] J. Bourquin, D. Septiadi, D. Vanhecke, S. Balog, L. Steinmetz, M. Spuch-Calvar, P. Taladriz-Blanco, A. Petri-Fink, B. Rothen-Rutishauser, *ACS Nano* **2019**, *13*, 7759.
[14] A. Saez, E. Anon, M. Ghibaudo, O. du Roure, J. M. Di Meglio, P. Hersen, P. Silberzan, A. Buguin, B. Ladoux, *J. Phys.: Condens. Matter* **2010**, *22*, 194119.
[15] O. du Roure, A. Saez, A. Buguin, R. H. Austin, P. Chavrier, P. Siberzan, B. Ladoux, *Proc. Natl. Acad. Sci. USA* **2005**, *102*, 2390.
[16] M. Morga, Z. Adamczyk, S. Godrich, M. Ocwieja, G. Papastavrou, *J. Colloid Interface Sci.* **2015**, *456*, 116.
[17] N. Goedecke, M. Bollhalder, R. Bernet, U. Silvan, J. Snedeker, *J. Vis. Exp.* **2015**, *17*, e53350.
[18] D. Septiadi, F. Crippa, T. L. Moore, B. Rothen-Rutishauser, A. Petri-Fink, *Adv. Mater.* **2018**, *30*, 1704463.
[19] A. Zareidoost, M. Yousefpour, B. Ghaseme, A. Amanzadeh, *J. Mater. Sci.: Mater. Med.* **2012**, *23*, 1479.
[20] D. Yamashita, M. Machigashira, M. Miyamoto, H. Takeuchi, K. Noguchi, Y. Izumi, S. Ban, *Dent. Mater. J.* **2009**, *28*, 461.
[21] F. Gentile, L. Tirinato, E. Battista, F. Causa, C. Liberale, E. M. di Fabrizio, P. Decuzzi, *Biomaterials* **2010**, *31*, 7205.
[22] B. Borm, R. P. Requardt, V. Herzog, G. Kirfel, *Exp. Cell Res.* **2005**, *302*, 83.
[23] B. Alberts, A. Johnson, J. Lewis, M. Raff, K. Roberts, P. Walter, *Molecular Biology of the Cell*, 4th ed., Garland Science, New York **2002**.
[24] L. M. Coluccio, L. G. Tilney, *J. Cell Biol.* **1984**, *99*, 529.
[25] J. A. Cooper, *J. Cell Biol.* **1987**, *105*, 1473.
[26] B. J. Iacopetta, E. H. Morgan, *J. Biol. Chem.* **1983**, *258*, 9108.
[27] J. Saraste, G. E. Palade, M. G. Farquhar, *Proc. Natl. Acad. Sci. USA* **1986**, *83*, 6425.
[28] T. dos Santos, J. Varela, I. Lynch, A. Salvati, K. A. Dawson, *PLoS One* **2011**, *6*, e24438.
[29] G. Giannelli, J. Falk-Marzillier, O. Schiraldi, W. G. Stetler-Stevenson, V. Quaranta, *Science* **1997**, *277*, 225.
[30] W. Stöber, A. Fink, E. Bohn, *J. Colloid Interface Sci.* **1968**, *26*, 62.
[31] T. L. Moore, D. Hauser, T. Gruber, B. Rothen-Rutishauser, M. Lattuada, A. Petri-Fink, R. Lyck, *ACS Appl. Mater. Interfaces* **2017**, *9*, 18501.
[32] D. R. Larson, H. Ow, H. D. Vishwasrao, A. A. Heikal, U. Wiesner, W. W. Webb, *Chem. Mater.* **2008**, *20*, 2677.
[33] S. Steiner, J. Czerwinski, P. Comte, O. Popovicheva, E. Kireeva, L. Müller, N. Heeb, A. Mayer, A. Fink, B. Rothen-Rutishauser, *Atmos. Environ.* **2013**, *81*, 380.
[34] E. M. Lifshitz, *Sov. Phys. JETP* **1956**, *2*, 73.
[35] F. Bordi, C. Cametti, G. Paradossi, *Biopolymers* **2000**, *53*, 129.
[36] J. Y. Tinevez, N. Perry, J. Schindelin, G. M. Hoopes, G. D. Reynolds, E. Laplantine, S. Y. Bednarek, S. L. Shorte, K. W. Eliceiri, *Methods* **2017**, *115*, 80.